Hindawi
Journal of Nanomaterials
Volume 2019, Article ID 7034620, 13 pages
https://doi.org/10.1155/2019/7034620

Research Article

Doping Efficiency in Cobalt-Doped ZnO Nanostructured Materials

Amrit Kaphle,[1] **Travis Reed**,[2] **Allen Apblett**,[2] **and Parameswar Hari**[1,3]

[1]*Department of Physics and Engineering Physics, University of Tulsa, Tulsa, Oklahoma 74104, USA*
[2]*Department of Chemistry, Oklahoma State University, Stillwater, Oklahoma 74078, USA*
[3]*Oklahoma Photovoltaic Research Institute, University of Tulsa, Tulsa, Oklahoma 74104, USA*

Correspondence should be addressed to Parameswar Hari; parameswar-harikumar@utulsa.edu

Received 8 November 2018; Revised 11 February 2019; Accepted 25 February 2019; Published 24 April 2019

Academic Editor: Ali Khorsand Zak

Nanostructured ZnO thin films doped with cobalt from 5% to 20% were grown on glass substrates by a low-temperature chemical bath deposition (CBD) technique. We compared the doping efficiency of incorporating cobalt in ZnO nanostructured samples doped with cobalt via cobalt nitrate and cobalt chloride. The concentration of cobalt incorporated into the ZnO matrix was precisely determined using inductively coupled plasma mass spectroscopy (ICP-MS). Scanning electron microscopy (SEM) images showed that only at a 0.1 M ratio of the precursor solutions in CBD using cobalt nitrate as a dopant, the morphology of ZnO yielded hexagonally shaped nanorods. At a 1 M ratio of the precursor solutions, SEM images showed that the morphology of ZnO was nanoplatelets at all doping levels, irrespective of the doping method used. The synthesized nanostructures retained the wurtzite hexagonal structure only at 0.1 M precursor solution using cobalt nitrate doping, which was confirmed by X-ray diffraction (XRD) studies. In cobalt-doped samples using cobalt chloride as a dopant, XRD analysis confirmed the formation of a Simonkolleite structure. At 300°C, the Simonkolleite structure was converted to a wurtzite structure without changing the morphology. Electrical conductivity measurements at 300 K showed that ZnO nanorods doped with cobalt using cobalt nitrate yielded the lowest resistivity. The molarity of the precursor solution and dopant was found to have a substantial impact on the morphology and doping efficiency of the ZnO nanostructures.

1. Introduction

Transparent semiconductors made of conductive oxides can provide antireflection coatings to facilitate higher absorption in solar cells. Currently, various nanostructured materials are studied for controlling light to increase absorption in photovoltaic (PV) cells. Zinc oxide has a wide range of useful optical and electronic properties which make it a promising material for optoelectronic devices. Recent studies show that optical, magnetic, and electrical properties of ZnO nanostructures can be controlled by defect centers and defect densities present in the ZnO lattice [1, 2]. Among transition metals, cobalt is a promising material for doping ZnO due to its similar ionic radius, abundant electronic states, and the divalent state [1, 3]. In addition, cobalt-doped ZnO samples exhibit remarkable optical and magnetic behavior even for small concentration of cobalt substitution in the ZnO structure (<2.0 at.%) [4]. Cobalt-doped ZnO thin films and nanostructures have been prepared by several deposition methods including sputtering, sol-gel, spin coating, solvothermal, ultrasonic spray, and pulsed laser deposition methods [5–10].

For developing a low-cost, scalable deposition method, for fabricating ZnO nanostructures, we used a chemical bath deposition (CBD) method that can easily incorporate metallic dopants. Our group has developed a scalable, low-temperature chemical bath deposition method by which the morphology, doping levels, and aspect ratio of the nanostructures can be easily controlled [11–14]. ZnO is known to exhibit a wide range of morphologies from nanowires and nanorods to plate-like structures [15]. A solution-based method to dope nanostructures with dopants such as cobalt, aluminum, cadmium, and manganese to tune the index of refraction as well as bandgap can be easily incorporated into

the CBD process. Doping of transition metals in ZnO results in bandgap reduction or enhancement depending on the dopant used [16, 17].

In this study, we report the dependence of doping on morphology, optical property, absorption, electrical conductivity, and photoluminescence (PL) of ZnO nanostructures doped with cobalt ranging from 5% to 20% grown on glass substrates. We have compared the doping efficiency in two sets of samples (0.1 M and 1 M of precursor solutions in CBD) doped with cobalt via cobalt nitrate and cobalt chloride.

2. Methods and Materials

Doped and undoped ZnO nanostructures were grown on a glass substrate by a chemical bath deposition (CBD) method. Zinc nitrate hexahydrate ($Zn(NO_3)_2{\cdot}6H_2O$, ≥99.5%), zinc chloride ($ZnCl_2$, ≥97%), cobalt nitrate hexahydrate ($Co(NO_3)_3{\cdot}6H_2O$, ≥98%), cobalt chloride hexahydrate ($CoCl_2{\cdot}6H_2O$, ≥98%), and hexamethylenetetramine ($C_6H_{12}N_4$, ≥98%) (HMTA) were purchased from Sigma-Aldrich (USA). Before deposition, glass substrates were cleaned with dilute hydrochloric acid, acetone, isopropanol, and deionized water.

Basic steps in fabricating ZnO nanostructures using the chemical bath deposition (CBD) are illustrated in Figure 1. ZnO Nanowire (NW) arrays were grown on a glass substrate using the CBD process we developed in the lab [11–14, 18–20]. The substrate was suspended vertically in an equimolar (0.1 M or 1 M) solution of zinc nitrate hexahydrate or zinc chloride and hexamethylenetetramine (HMTA), which were used as precursors. The reaction was carried out for 6 hours at 95°C in an oven. The vertically grown nanostructures were annealed at 300°C for an hour. To fabricate ZnO nanostructures doped with cobalt, either cobalt chloride or cobalt nitrate with different Co/Zn molar ratios was added to the chemical bath precursor solution.

2.1. Characterizations. Structural characterization of prepared ZnO nanostructures on glass substrates was done with an FEI Inspect S50 scanning electron microscope (SEM). The X-ray diffraction pattern for the ZnO nanostructures was recorded using an X-ray diffractometer (CuKα radiation, $\lambda = 1.54056$ A^0). Dopant concentrations were analytically determined using an ELAN DRC II ICP Mass Spectrometer. The absorption spectra of samples were measured with a Varian Cary 50 Scan UV-Vis spectrometer. Photoluminescence (PL) was measured using a Jasco FP-6500 Spectrofluorometer. Electrical conductivity was measured using MMR H-50 Hall (Van der Pauw) equipped with a cryostat.

3. Results and Discussions

3.1. Inductively Coupled Plasma Mass Spectroscopy (ICP-MS) Studies. The percentage of cobalt incorporated into the doped samples was measured using inductively coupled plasma mass spectroscopy (ICP-MS). Table 1 summarizes the ICP-MS results. By comparing the measured cobalt percentage from deposited films to the estimated cobalt percentage

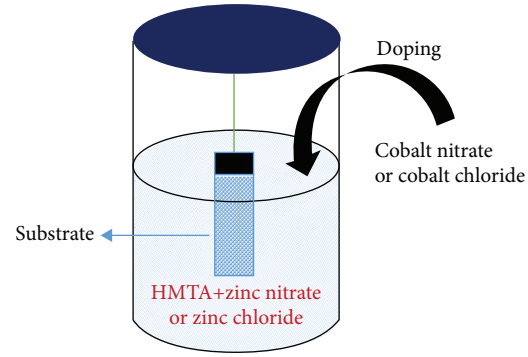

Figure 1: Chemical bath deposition (CBD) method for growing ZnO nanostructures.

Table 1: ICP-MS results for 5% to 20% cobalt-doped ZnO samples.

Co % (expected)	ICP-MS results (%)			
	Cobalt nitrate		Cobalt chloride	
	0.1 M	1 M	0.1 M	1 M
5	1.07 ± 0.43	3.38 ± 0.27	3.28 ± 0.26	4.49 ± 0.32
10	3.13 ± 0.38	7.06 ± 0.25	9.17 ± 0.23	9.30 ± 0.28
15	6.18 ± 0.34	11.10 ± 0.22	12.60 ± 0.19	14.68 ± 0.27
20	9.08 ± 0.29	14.83 ± 0.22	20.63 ± 0.17	19.08 ± 0.24

based on stoichiometry, the cobalt percentage in ZnO samples doped with cobalt chloride matches better than the cobalt content in ZnO nanostructures doped with cobalt nitrate. These differences might be due to the solubility of cobalt in the zinc hydroxide host lattice. It is well known that during the doping process, cobalt adopts the tetrahedral sites such as $(OH)_4$ sites in the nitrate precursor and $(OH)_3Cl$ in the chloride precursor [21, 22]. Thus, we believe that Co^{++} ions most likely favored to incorporate into tetrahedral $(OH)_3Cl$ sites rather than tetrahedral $(OH)_4$ in comparison to the Zn^{++} leading to the low incorporation of Co^{++} in the nitrate route of doping.

According to the growth mechanisms of nanostructures using two different routes, which will be discussed later, the incorporation of cobalt into the ZnO nanostructure can be described as follows. For nitrate salt with low molar concentration, the growth is along the *c*-axis (nanorods). Zinc and cobalt are mostly in the form of Zn^{++} ions and some cobalt complexes, respectively. There are no preferential electrostatic interactions between the surfaces of the ZnO nanorods and the different complexes in aqueous solution for low concentration [23]. So the chances of cobalt incorporation are low. This was seen in ICP-MS analysis results as actual cobalt incorporation is very low for 0.1 M concentration than the expected cobalt concentration. As the concentration of nitrate salts is increased (1 M) and the precursor solution of chloride is used (0.1 M and 1 M), both cases give rise to the formation of 2D nanostructures. Therefore, as growth proceeds, more negative $Co(OH)_2$ complexes are adsorbed on the positive surfaces of 2D ZnO nanostructures and act as capping agents to inhibit their development, favoring the cobalt uniform incorporation into ZnO. This type of face-

selective electrostatic control in the CBD method is discussed earlier by Joo et al. [24] for aluminum-doped ZnO nanostructures. On the other hand, chloride as precursor salts gives rise to the formation of additional $Co_2(OH)_3Cl$ complexes [25] which are absorbed by the positive surface of ZnO nanosheets. As a result, a significant amount of cobalt is incorporated into ZnO nanostructures following the possible dissociation of more $Co(OH)_2$ and $Co_2(OH)_3Cl$ complexes during growth and subsequently as the annealing at 300°C is accomplished. A similar type of mechanism was discussed by Verrier et al. [23, 26] and Winkler et al. [27] for aluminum- and magnesium-doped ZnO nanostructure, respectively. Based on these arguments, we can say that cobalt percentage in ZnO nanostructures doped with the cobalt chloride route matches better than the cobalt content in ZnO nanostructures doped with the cobalt nitrate route.

3.2. Morphology and Growth Mechanism. Morphological variations in cobalt-doped ZnO nanostructures were measured using SEM. Figure 2 shows the typical morphology of ZnO nanostructured films at 0.1 and 1.0 molarities in 10% cobalt-doped ZnO via cobalt chloride and cobalt nitrate. As it is evident from these images, cobalt doping via nitrate preserves the nanorod structure at 0.1 M. Figures 3(a) and 3(b) show the undoped and 5% cobalt-doped ZnO nanorods. As the doping level is increased, we observe an increase in ZnO nanorod diameter (Figure 3(c)) with cobalt concentration doped via cobalt nitrate (0.1 M). This can be explained as cobalt can create a complex with hydroxide during the growth process, which reduced the reaction between Zn^{++} and OH^- ions altering the overall nucleation process. This mechanism can promote lateral growth rather than perpendicular growth; as a result, the diameter of nanorods increases [20, 28]. At a 1 M ratio of the precursor solutions, SEM images show a morphological pattern in the form of platelets at all doping levels, irrespective of the doping method used (Figures 2(b) and 2(d)).

The set of overall reactions most often referenced in the literature for ZnO deposition from $Zn(NO_3)_2$ and HMTA precursors at 95°C is [29–31]

$$(CH_2)_6N_4 + 6H_2O \rightarrow 6HCHO + 4NH_3, \quad (1)$$

$$NH_3 + H_2O \leftrightarrows NH_4^+ + OH^-, \quad (2)$$

$$2OH^- + Zn^{++} \leftrightarrows Zn(OH)_2, \quad (3)$$

$$Zn(OH)_2 \rightarrow ZnO + H_2O. \quad (4)$$

First, HMTA decomposes upon heating to form formaldehyde and ammonia (equation (1)). Ammonia reacts with water to produce OH^- (equation (2)), which energizes the crystallization of ZnO (equations (3) and (4)), which is nonsoluble, and therefore precipitates homogeneously and heterogeneously if a substrate is present in the precursor solution. It has been suggested in many works of literature that $Zn(OH)_2$ forms before the growth of ZnO, which then grows through a dissolution and reprecipitation mechanism, where $Zn(OH)_2$ acts as a reservoir of zinc [31]. ZnO, not $Zn(OH)_2$, forms as the final product because of the pH of the solution, which is buffered by HMTA [31]. The morphology of the as-synthesized ZnO nanostructures strongly depends on the experimental conditions, particularly the concentration of Zn^{++} ions, which might change the reaction rate of the hydroxylation (equation (3)) and dehydration (equation (4)), thereby enabling the adaptation of the growth behavior of ZnO nanostructures [32, 33].

The dehydration reaction plays an essential role in the precursor solution containing a low concentration of Zn^{++} ions [32, 34]. Thus, $Zn(OH)_2$ can be converted into ZnO as soon as it is produced, leading to the formation of one-dimensional ZnO nanostructures such as nanorods (Figure 2(c)) because of the anisotropic growth along the (0001) direction of the hexagonal wurtzite structure. When the concentration of the precursor solution is high, dehydration of $Zn(OH)_2$ could be delayed because of the relatively faster hydroxylation reaction due to the high concentration of Zn^{++} ions [33]. As a result, the growth along the (0001) direction or *c*-axis might be changed to the other preferred growth direction, such as $(01\bar{1}0)$ and $(10\bar{1}0)$ [34, 35], which can give rise to the formation of 2D nanostructures such as nanosheets or closely packed bunches [34, 36]. Therefore, at very high concentration of precursor solution, the quantity of Zn^{++} ions derived from the precursor will increase, thus generating more nucleation sites, and aggregate and eventually will lead to the very dense growth of nanostructures (closely packed bunches (Figure 2(d))).

In the case of the chloride precursor, we believe that the capping effect plays a key role in the anisotropic growth of ZnO nanostructures due to excessive Cl^- ions (equation (5)). When we used $ZnCl_2$ as the precursor solution, Cl^- ions would be adsorbed preferentially on the positive polar face of the (0001) surface, which prevented the contact of $Zn(OH)_4^{2-}$ on the (0001) surface and thus limited the crystal growth along the *c*-axis, redirecting the growth along other nonpolar direction. The resulting nanostructures, therefore, have the preferred growth direction of $(10\bar{1}0)$ and appear as a 2D plate-like structure, as illustrated in Figure 2(a). It should be noted that while we expect that similar adsorption of Cl^- ions would have occurred on the polar (0001) plane in the case of high concentration, the slow hydroxylation kinetics allows sufficient time for ion exchange, hence preventing significant surface capping by Cl^- ions. However, at a sufficiently high concentration (1 M), a more capping effect of Cl^- will take place which increases nanostructure size. Additionally, in the case of $ZnCl_2$, the formation of HCl as a byproduct occurs during the growth process. According to Smith and Rodriguez-Clemente [37], HCl vapor molecules act as a capping agent during the film growth by lowering the specific surface energy of polar faces; this slows down their growth and controls the shape of the nanostructures. Similar results [34, 38] were reported by using potassium chloride (KCl) electrolyte for the growth of ZnO nanostructures.

$$Zn^{++} + x(OH)^- + yCl^- \rightarrow Zn(OH)_xCl_y. \quad (5)$$

3.3. X-Ray Diffraction (XRD) Studies. XRD images of cobalt-doped ZnO nanostructures with different doping

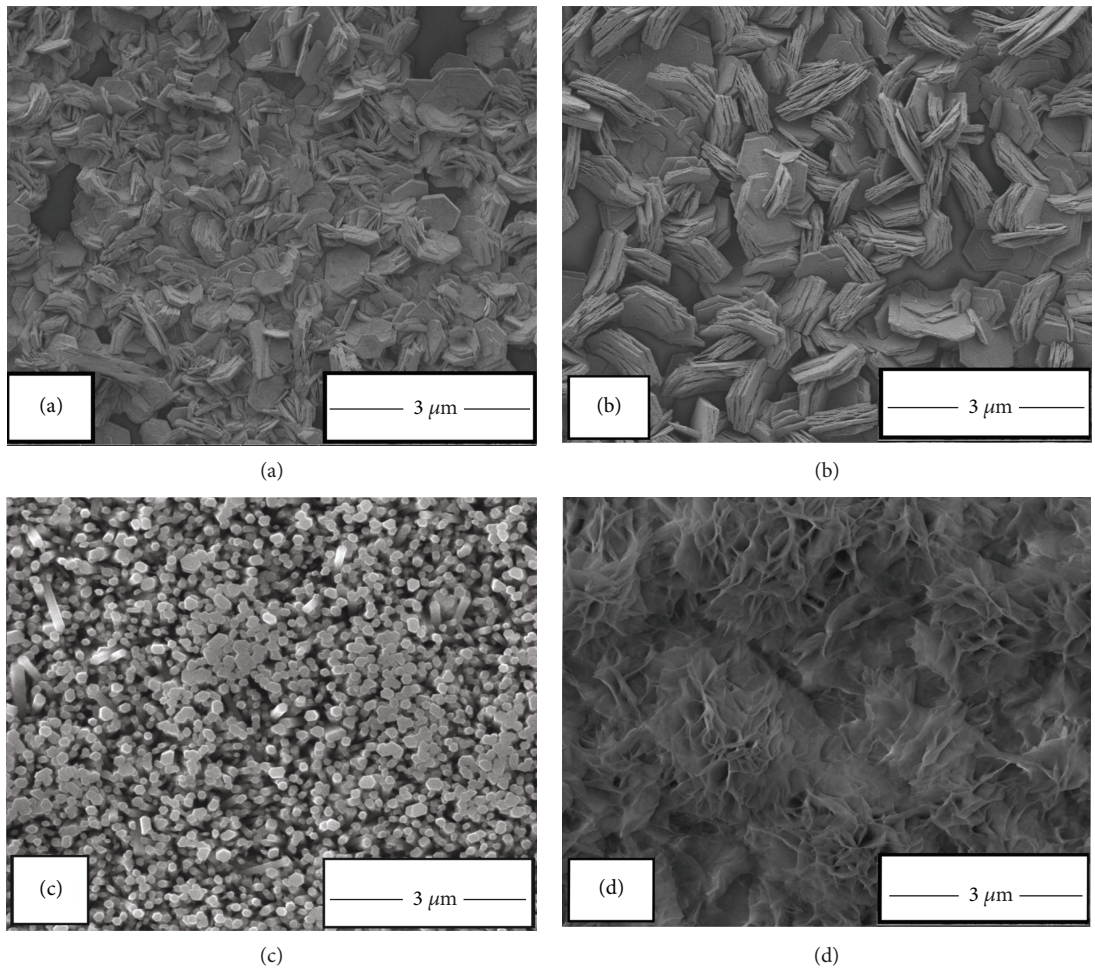

Figure 2: SEM images of 10% cobalt-doped ZnO nanostructures via cobalt chloride ((a) 0.1 M precursor and (b) 1 M precursor) and cobalt nitrate ((c) 0.1 M precursor and (d) 1 M precursor).

concentrations are shown in Figure 4. For 0.1 M cobalt nitrate-doped samples, all the peaks match well with the hexagonal wurtzite structure of ZnO (JCPDS card 79-2205). As no peaks are indicating the presence of cobalt metal clusters as well as cobalt oxides, cobalt ions are incorporated into the ZnO lattice without changing the wurtzite structure of the ZnO. With an increase in the cobalt concentration, the preferential growth along the *c*-axis becomes more and more observable in ZnO nanostructures (Figures 4(a) and 4(c)). For 1 M cobalt nitrate-doped samples, the XRD image was confirmed to be of zinc hydroxide nitrate ($Zn_5(OH)_8(NO_3)_2{\cdot}2H_2O$, JCPDS card 24-1460). Similarly, for cobalt chloride-doped samples (0.1 M and 1 M), the product was confirmed to be Simonkolleite or zinc chloride hydroxide monohydrate ($Zn_5(OH)_8Cl_2{\cdot}H_2O$, JCPDS card 07-0155) as shown in Figure 4(b). From XRD data, it appears that the growth is more reinforced within the basal direction rather than the transverse direction at higher molarity using the nitrate salt as well as the chloride salt. This type of growth pattern might originate from the hexagonal facet in nucleation and subsequent layer growth mode like Frank-van der Merwe-driven process along the (003) plane [39]. We can also infer that the high concentration of nitrate and chloride ions favors the formation of the layered hydroxide structure. By calcination, the Simonkolleite structure is initially converted into zinc oxide by releasing HCl and H_2O as

$$Zn_5(OH)_8Cl_2 \cdot H_2O \rightarrow^{300^\circ C} 5ZnO + 2HCl + 4H_2O. \quad (6)$$

By annealing the samples at 300°C in the air for 2 hours, the Simonkolleite phase is transformed into the pure ZnO phase as shown in Figure 4(c). However, SEM analysis revealed that the transformed ZnO phase completely maintains the platelet morphology of Simonkolleite even after annealing at 300°C. Similarly, by annealing at 300°C in the air for 2 hours, the zinc hydroxide nitrate structure is converted into the pure ZnO phase as

$$Zn_5(OH)_8(NO_3)_2 \cdot 2H_2O \rightarrow^{300^\circ C} 5ZnO + 2HNO_3 + 5H_2O. \quad (7)$$

3.4. Optical Studies. Optical measurements in cobalt-doped ZnO nanostructures were performed using a UV-Vis Cary

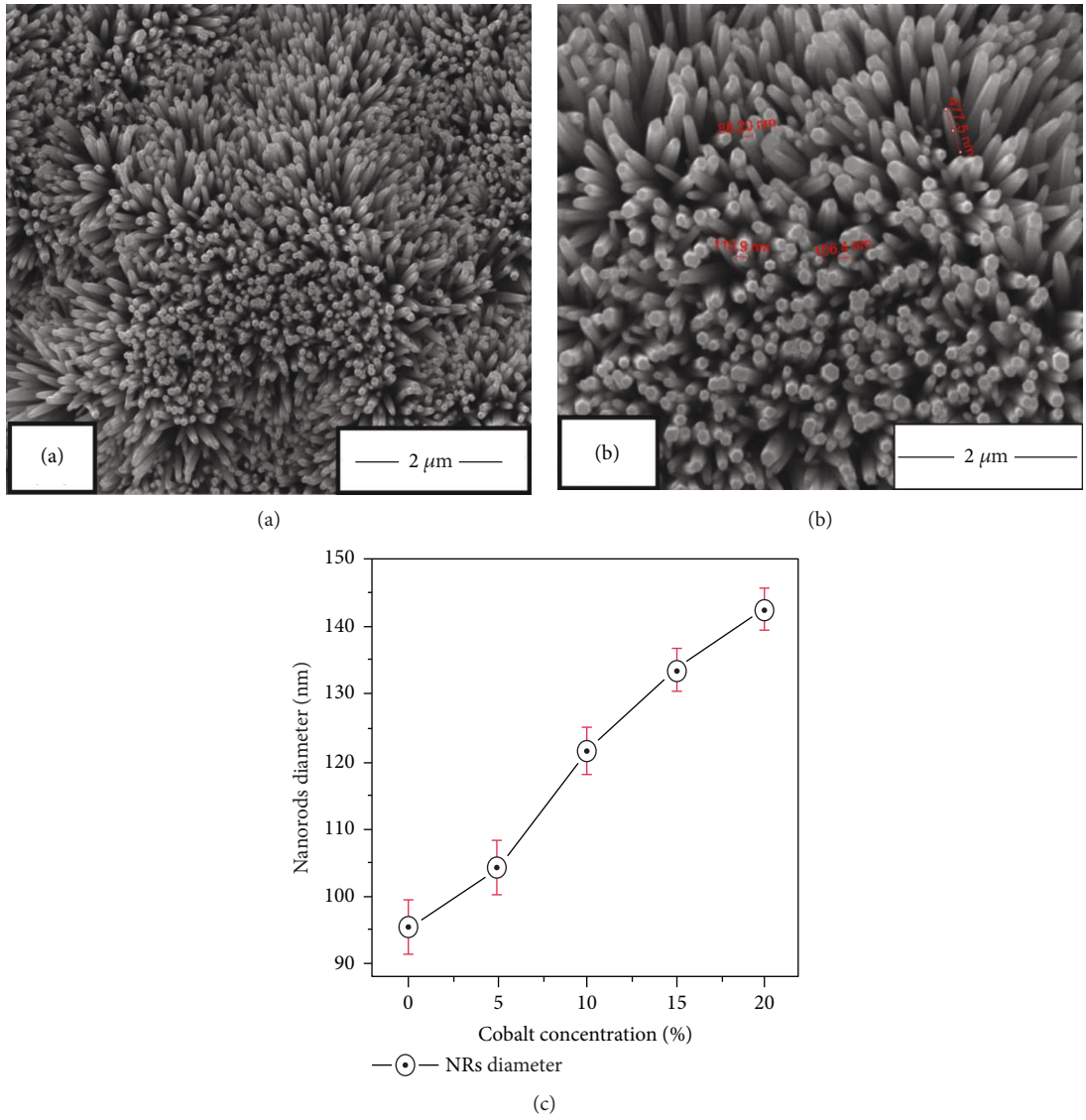

FIGURE 3: SEM images of nanorods at 0.1 M precursor using cobalt nitrate as doping: (a) 0% and (b) 5%. (c) Variation in size of ZnO nanorods with doping (0.1 M nitrate).

50 spectrometer. Figure 5 shows the optical absorption spectra of cobalt-doped ZnO nanostructures at room temperature for the nanostructures grown at various cobalt concentrations (doped with either cobalt nitrate or cobalt chloride). For all doped nanostructures, the absorption intensity increased and absorption peaks shifted towards longer wavelengths. With cobalt doping, the absorption spectra became broader after the UV peak observed at 385 nm, which might have been caused by surface-related defects in nanostructured ZnO [40–42].

The bandgap of ZnO nanostructured films can be estimated by applying the Tauc relationship using the following expression [43]:

$$\alpha h\nu = C\left(h\nu - E_g\right)^{1/2}, \tag{8}$$

where E_g is the bandgap energy, C is an energy-independent constant, and α is the absorption coefficient calculated using the following relation:

$$\alpha = \frac{2.303A}{t}, \tag{9}$$

where A is the absorbance and t is the thickness of the ZnO films.

The optical bandgap was determined by extrapolating the linear region in the $(\alpha h\nu)^2$ versus $h\nu$ plot to the horizontal axis. Figures 6(a) and 6(b) show the plots of $(\alpha h\nu)^2$ versus photon energy for the 0% and 15% cobalt-doped ZnO nanorods. Regardless of the route taken to achieve doping, the bandgap in cobalt-doped ZnO decreases with doping as shown in Figure 6(c). Bandgap shift was more pronounced

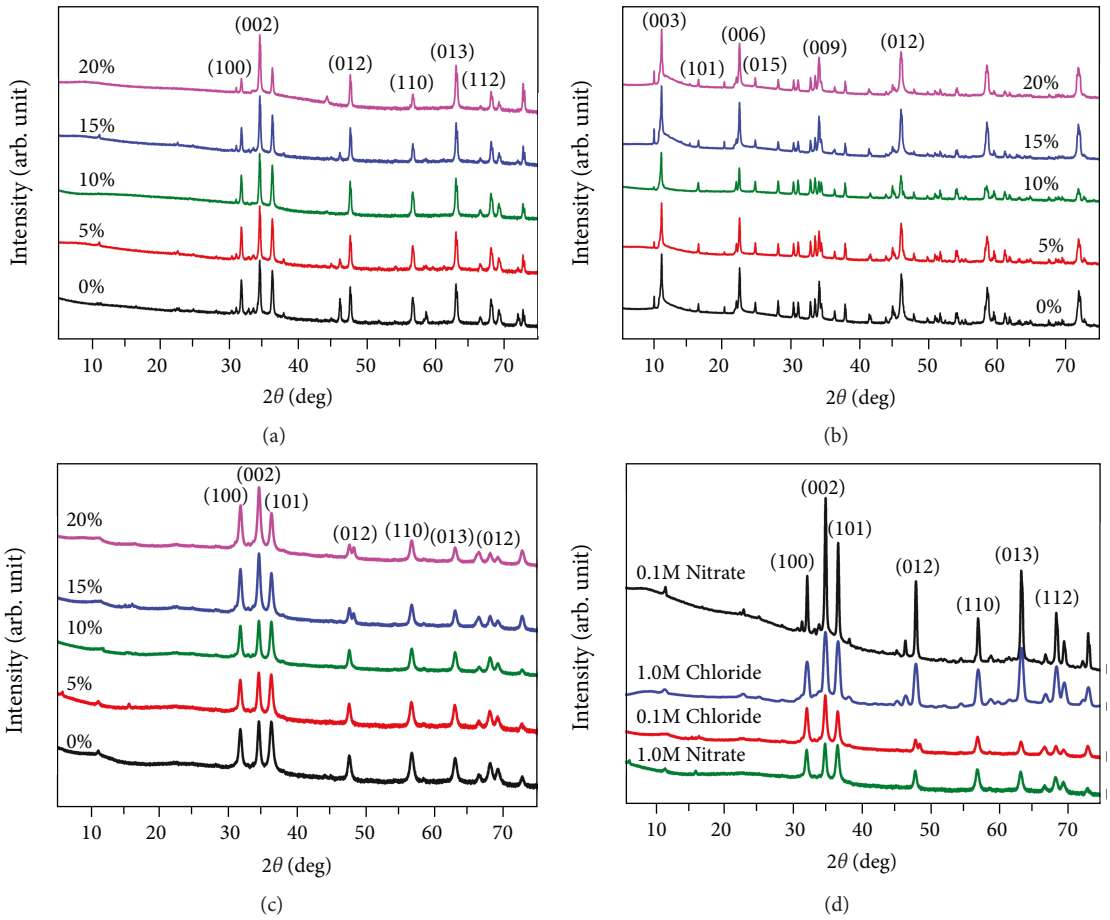

Figure 4: X-ray diffraction (XRD) pattern of (a) 0.1 M cobalt nitrate-doped samples, (b) 0.1 M cobalt chloride-doped samples, (c) 0.1 M cobalt chloride-doped samples annealed at 300°C, and (d) 15% cobalt-doped ZnO after annealing at 300°C with different precursors and concentrations. Evidence of the Simonkolleite phase, $Zn_5(OH)_8Cl_2{\cdot}H_2O$, in cobalt chloride-doped ZnO is shown in (b).

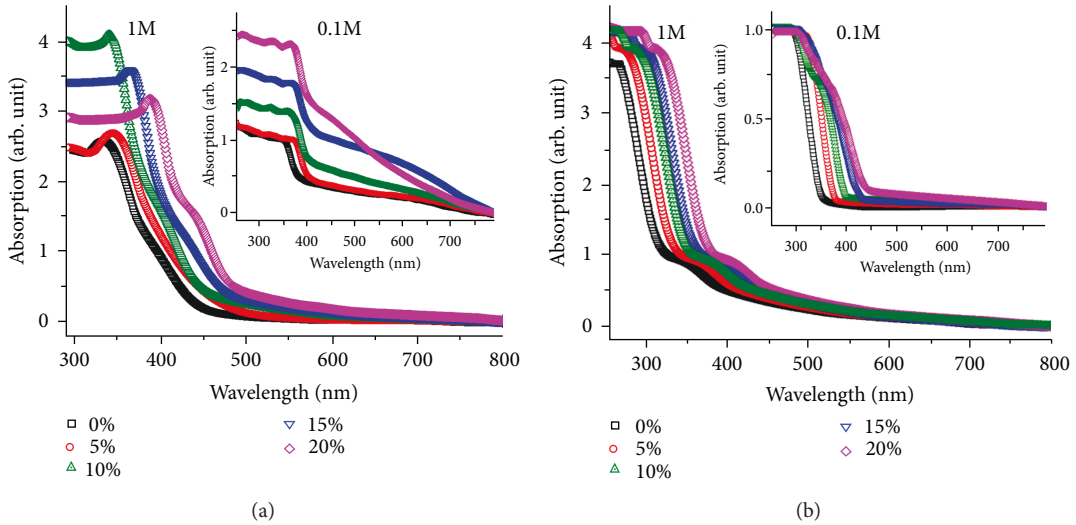

Figure 5: Absorption spectra of 0-20% cobalt-doped ZnO nanostructures: (a) 1 M precursor using nitrate (inset shows 0.1 M precursor using nitrate) and (b) 1 M precursor using chloride (inset shows 0.1 M precursor using chloride).

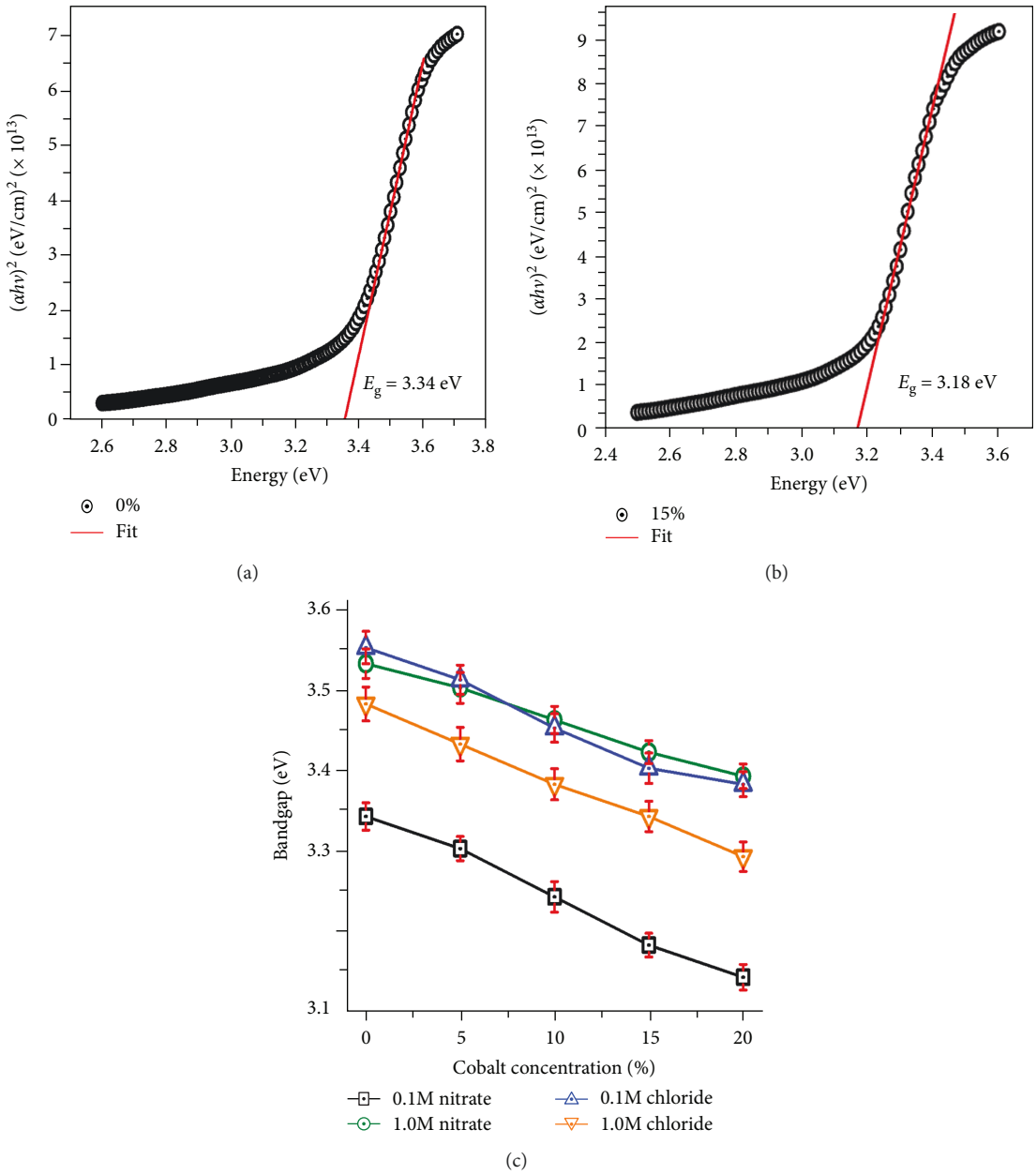

Figure 6: Tauc plot to calculate the bandgap of (a) 0% and (b) 15% cobalt-doped ZnO at 0.1 M precursor using cobalt nitrate. (c) Bandgap variation with cobalt doping for different precursor concentrations.

in 0.1 M cobalt nitrate-doped samples. A redshift of the optical bandgap with the incorporation of cobalt into ZnO has been reported and explained as being mainly due to sp-d exchange interactions between the band electrons and the localized d-electrons of the Co^{++} substituting for Zn^{++} ions [44, 45]. Exchange interaction is expected to contribute a negative and a positive correction to the conduction and valence band, respectively, causing the bandgap to shrink [46]. Previous studies also observed a redshift in the bandgap energy as the cobalt concentration is increased [20, 47–49]. Kim and Park [46] reported that with increasing cobalt concentration from 0% to 10%, the bandgap decreases in cobalt-doped samples. Ivill et al. [50] deposited a ZnO thin film with cobalt doping from 0% to 30% by a pulsed laser deposition technique and showed that the bandgap value increased from 3.28 eV to 3.80 eV. Ozerov et al. [51] also reported a blueshift in the bandgap in monocrystalline ZnO films. Yoo et al. [52] observed a blueshift in aluminum- and cobalt-doped ZnO films which were attributed to the Burstein–Moss effect from an increase in the carrier concentration [50]. The wide range of trends in bandgap with cobalt doping reported in the literature might be due to specific deposition and annealing conditions used in preparing doped ZnO samples.

We observed that the bandgap of ZnO for 1 M nitrate is greater than that for 0.1 M nitrate, but in the case of chloride, this is opposite in trend. From XRD result (Figure 4(d)), it is

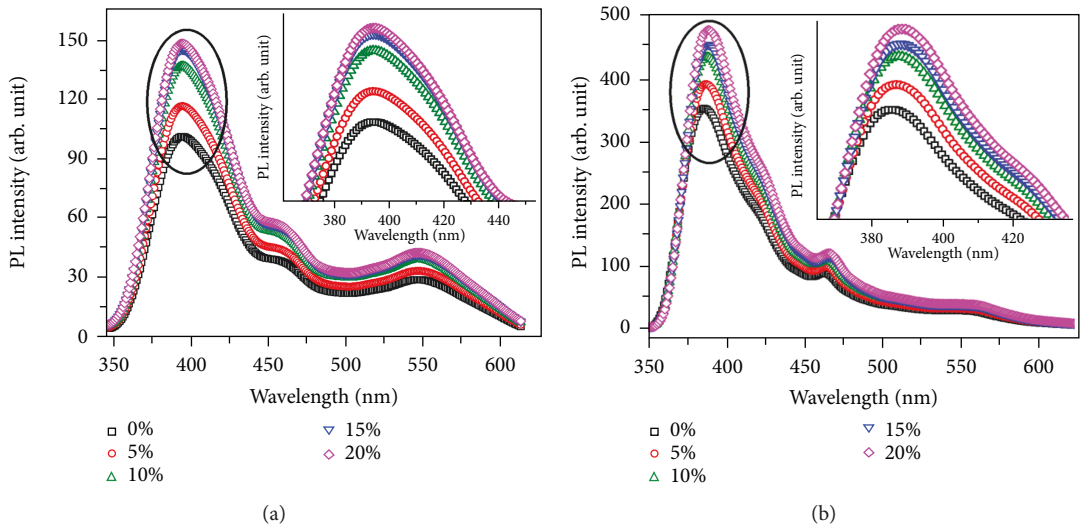

Figure 7: Photoluminescence (PL) spectra of cobalt-doped ZnO samples: (a) 0.1 M precursor with cobalt nitrate doping and (b) 0.1 M precursor with cobalt chloride doping. The inset shows the magnified area of the near band edge (NBE) peak.

confirmed that crystallinity of ZnO nanostructures is highest for 0.1 M nitrate as compared to chloride. It is known that the ZnO lattice structure has a limited capacity for substitution of Co^{++} ions. Therefore, the excess Co atoms, more than lattice capacity, go to the interstitial positions. It means that there are limited substitutional and extreme interstitial positions for Co^{++} for 1 M nitrate and both 0.1 M and 1 M for chloride route. In the case of the chloride precursor, the 0.1 M sample has more crystallinity than the 1 M sample because of the substitution of more Co^{++} ions into ZnO lattice with less interstitial defects. Therefore, we believe that the ZnO nanostructure from 0.1 M chloride route has relatively more crystallinity than that from 1 M chloride source. Samples with a more crystallized phase have smaller bandgap values.

Figure 7 shows the results from photoluminescence (PL) measurements at room temperature in the two sets of cobalt-doped samples, prepared at two different molarities, doped with cobalt nitrate and cobalt chloride. PL spectra confirmed that all ZnO films exhibited three distinct peaks: one in the UV range and the other two in the visible range as shown in Figures 7(a) and 7(b). The peak in the UV region corresponds to the near band edge, attributed to the radiative recombination of free excitons, and the peaks in the visible region are associated with structural defects such as zinc interstitials and oxygen vacancies [53]. In both cobalt nitrate and cobalt chloride doping, PL spectra show near band edge (NBE) peak shift to a longer wavelength as shown in Figure 8. This UV PL emission peak corresponds to the band edge emission of ZnO nanostructures. This NBE peak is redshifted from 394.24 nm to 396.03 nm for 0.1 M nitrate, 386.82 to 389.55 nm for 1 M nitrate, 384.23 to 386.83 nm for 0.1 M chloride, and 383.37 to 386.68 nm for 1 M chloride samples as the cobalt concentration increases from 0% to 20%. The observed redshift in the PL emission spectra may arise due to the increase in nanostructure size, as well as due to the reduction of the bandgap of the samples with increasing

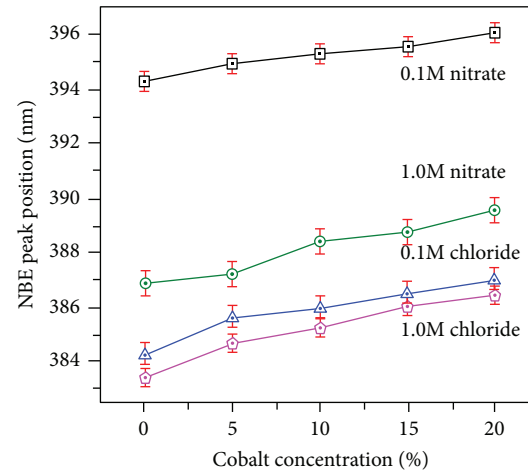

Figure 8: Variation in NBE peak position with cobalt doping (nitrate and chloride) for different precursor concentrations.

cobalt doping. However, the stress developed in the samples during the growth of nanostructures as well as doping may also play a significant role in shifting the PL emission peak [54].

Similar redshift in PL emission in ZnO NPs has been reported earlier by Sendi and Mahmud [55]. A strong redshift in UV PL spectra of cobalt-doped ZnO nanorods was also observed by Ghosh et al. [56].

It can be observed that for both 0.1 M and 1 M nitrate samples when compared to the undoped sample, the intensity of the defect peak increased with cobalt doping, which has already been reported in earlier studies [57, 58]. An increase in the intensity of the defect peak (460 nm and 545 nm) indicates the increase in the density of zinc interstitials and oxygen vacancies with doping as the doping concentration increases from 5% to 20%.

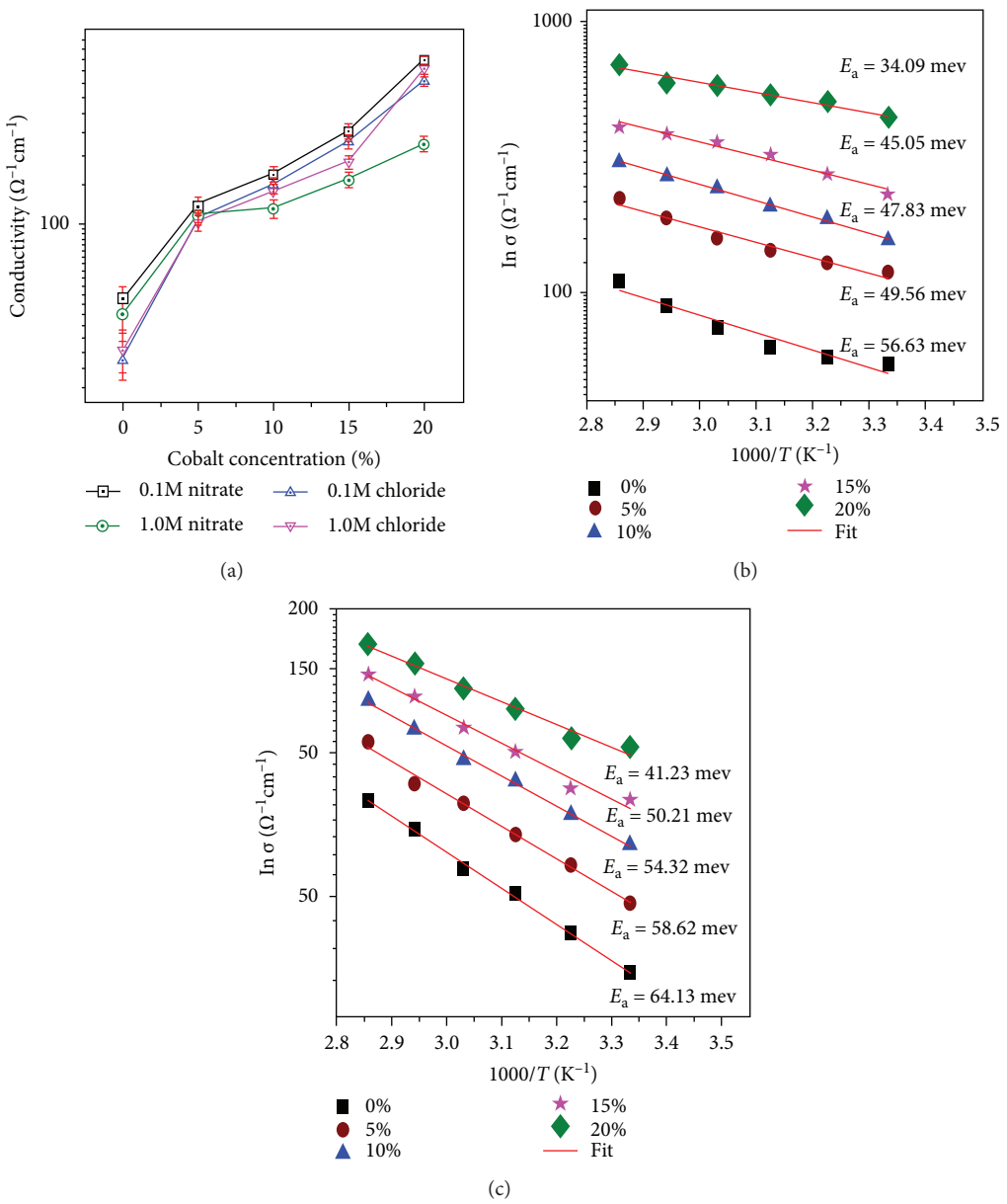

FIGURE 9: Variation of conductivity in doped samples (a) for two routes (0.1 M and 1 M) with temperature for (b) 0.1 M cobalt nitrate and (c) 1 M cobalt chloride. The slope of a linear fit gives the estimate for thermal activation energy.

3.5. Conductivity Measurements. We also performed four-point electrical conductivity measurements on cobalt-doped ZnO samples as a function of temperature. Figure 9(a) summarizes the conductivity variation in doped ZnO samples with temperature in 0-20% cobalt. As it is evident from the figure, the conductivity increases with the increase in doping concentrations. This increase in conduction could be explained by the improvement of crystallinity and enhanced substitution doping. As doping increases, grain size increases and it reduces the charge carrier scattering at grain boundaries, and hence, there is an increase in mobility as well as conductivity [59]. Wu et al. [60] prepared cobalt-doped ZnO (0%-10%) by the sol-gel method and showed that the substitution of Co^{++} for Zn^{++} could improve the electrical conductivity due to the increase in carrier concentration. In addition, we estimated several activation energies using equation (5), indicative of various conduction mechanisms involved in the doped samples. Figures 9(b) and 9(c) show the variation in conductivity with temperature and doping. For thermally activated band conduction, the conductivity can be expressed as [61, 62]

$$\sigma = \sigma_0 \exp\left(\frac{-E}{k_B T}\right), \tag{10}$$

where σ_0 is a constant, E is the activation energy, and k_B is Boltzmann's constant.

Cobalt doping increases the electron concentration, which in turn enhances the electrical conductivity with doping. The activation energy measured from conductivity for the undoped ZnO (0.1 M nitrate) was 56.63 meV, which is very close to the exciton binding energy (60 meV) of ZnO. The decrease in activation energy with cobalt doping indicates that less and less energy will be required for carriers to jump to higher electronic states. Yousif et al. [63] reported that the activation energy of cobalt-doped ZnO increases up to 3% and then decreased with a further increase in cobalt doping. The activation energy for the thermally stimulated conduction band depends on the donor carrier density and the impurity energy levels. An increase in donor carrier density brings the Fermi level up in the bandgap, which results in a decrease in activation energy [61, 64]. Table 2 shows the values of activation energies estimated from conductivity measurements for different cobalt-doped samples with 0.1 M and 1 M molarities.

3.6. Doping Efficiency. One of the observations from our optical measurements in doped ZnO is that bandgap reduces in doped samples as the doping concentration is increased. This effect could be explained by the wave functions of the electrons bound to the impurity atoms that start to overlap as the density of the impurities increases. As a result, this overlap forces the energies to form an energy band rather than a discreet level [65]. This impurity band, in turn, reduces the effective energy bandgap of the host material. The shift bandgap (ΔE_g) is given as [65]

$$\Delta E_g = \frac{3q^2}{16\pi\varepsilon_s}\sqrt{\frac{q^2 N_d}{\varepsilon_s kT}}, \tag{11}$$

where N_d is the doping density, q is the electronic charge, ε_s is the dielectric constant of the semiconductor, k is Boltzmann's constant, and T is the room temperature. For ZnO, $\varepsilon_s = 8.75$ [66]. The doping density is estimated using equation (11) and is shown in Table 3 for various cobalt-doped samples. The ICP-MS result shows that there is a significant discrepancy between the expected and actual measured cobalt percentage in various cobalt-doped ZnO samples. This is an indication of the large difference in doping efficiency, i.e., the percentage of cobalt atom which effectively donates a free electron to the ZnO matrix. With one Co atom donating at maximum one free electron, the doping efficiency can be measured by [67]

$$\begin{aligned}\eta &= \frac{\text{atomic density of active dopant}}{\text{atomic density of cobalt}} \times 100\% \\ &= \frac{n - n_0}{N_{Zn} \times \text{CF}} \times 100\%,\end{aligned} \tag{12}$$

where n and n_0 are the charge carrier densities of cobalt-doped and undoped ZnO, respectively. N_{Zn} is the atomic density of Zn which is 4.0×10^{22} cm^{-3}, $n - n_0$ is the active dopant density, and CF is the cobalt fraction or doping level (shown in Table 1) which was calculated from the atomic fraction of cobalt (Co atom %) and zinc (Zn atom %) as measured by ICP-MS [67]. Results are shown in Table 3. Doping efficiency of cobalt-doped ZnO with different molarities is shown in Figure 10. At 0.1 M concentration, the doping efficiency with cobalt chloride is almost 2.5-4.5 times higher than the doping efficiency using cobalt nitrate. Also, at a higher molar concentration (1 M), doping via cobalt chloride is about 1.6-1.9 times more efficient than doping via cobalt nitrate. Based on the doping efficiency estimates, cobalt incorporation into ZnO is much more efficient at a 1 M concentration of the precursor solution using cobalt chloride. However, control of the molarity of the precursor components allows us to prepare selectively either sheet-like layered hydroxide (zinc hydroxide nitrate and zinc hydroxide chloride) or pure zinc oxide nanorods.

Table 2: Activation energies for different cobalt-doped ZnO.

Co %	Activation energy (meV)			
	Cobalt nitrate-doped ZnO		Cobalt chloride-doped ZnO	
	0.1 M	1 M	0.1 M	1 M
0	56.63	63.51	66.63	64.13
5	49.56	59.32	61.29	58.62
10	47.83	56.05	57.08	54.32
15	45.05	52.58	52.87	50.21
20	34.09	46.39	49.16	41.23

4. Conclusion

Zinc oxide (ZnO) nanostructures doped with cobalt from 5% to 20% were grown by a chemical bath deposition technique. From structural studies, only when we use cobalt nitrate as a dopant (0.1 M), we observe well-aligned ZnO nanorod growth. At a 1 M ratio of the precursor solutions, SEM images show that the morphology revealed nanoplatelets at all doping levels, irrespective of the doping method used. The X-ray diffraction study confirmed that the prepared particles were of the hexagonal wurtzite structure only at 0.1 M of precursors using cobalt nitrate as doping salt. Therefore, careful control of the molarity of the precursor allows us to prepare selectively layered hydroxide (zinc hydroxide nitrate and zinc hydroxide chloride) and pure zinc oxide nanorods. The Simonkolleite and zinc hydroxide nitrate structures were converted to highly .oriented polycrystalline zinc oxide sheets by annealing at 300°C for 2 hours in the air. Optical absorption measurements were conducted, and the bandgap was estimated in various doped samples. One significant result of our study is that regardless of the route taken to achieve doping, the bandgap decreases with doping. PL spectra of the doped samples show a peak shift to longer wavelengths in both cobalt chloride and cobalt nitrate samples. In both cobalt chloride- and cobalt nitrate-doped ZnO, conductivity increased with doping. Variations in conductivity are more significant in cobalt nitrate-doped ZnO when compared to cobalt chloride-doped ZnO. Based on the cobalt incorporation efficiency, doping of ZnO with cobalt chloride may be a better method

Table 3: Bandgap shrinkage, doping concentration, and doping efficiency for cobalt nitrate- and cobalt chloride-doped ZnO nanostructures at 0.1 M and 1 M molarities.

Co %	Cobalt nitrate-doped ZnO						Cobalt chloride-doped ZnO					
	0.1 M			1 M			0.1 M			1 M		
	ΔE_g (eV)	N_d (cm^{-3})	η (%)	ΔE_g (eV)	N_d (cm^{-3})	η (%)	ΔE_g (eV)	N_d (cm^{-3})	η (%)	ΔE_g (eV)	N_d (cm^{-3})	η (%)
5	-0.04	2.14×10^{20}	5.01	-0.03	1.21×10^{20}	9.79	-0.04	2.14×10^{20}	12.51	-0.04	2.14×10^{20}	18.66
10	-0.10	1.34×10^{21}	10.71	-0.07	6.56×10^{20}	23.25	-0.10	1.34×10^{21}	36.54	-0.11	1.48×10^{21}	39.72
15	-0.16	3.43×10^{21}	13.88	-0.11	1.63×10^{21}	36.53	-0.14	2.62×10^{21}	52.13	-0.16	3.43×10^{21}	58.44
20	-0.20	5.36×10^{21}	14.76	-0.14	2.62×10^{21}	44.29	-0.20	5.36×10^{21}	64.98	-0.20	5.36×10^{21}	70.25

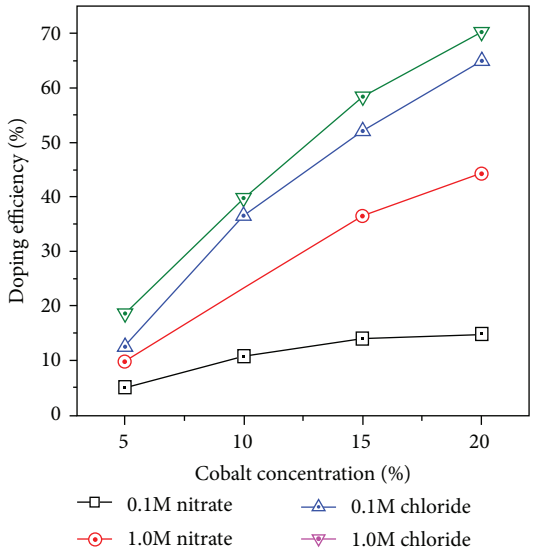

Figure 10: Doping efficiency of cobalt-doped ZnO nanostructures as a function of cobalt concentration.

for achieving higher doping efficiency by a chemical bath deposition method.

Data Availability

The data used to support the findings of this study are available from the corresponding author upon request.

Conflicts of Interest

The authors declare that there is no conflict of interest regarding the publication of this paper.

Acknowledgments

This work was supported by NASA EPSCoR (grant numbers NNX13AN01A and NNX15AM75A). The authors would like to acknowledge Dr. Kenneth Roberts, Dr. Alexie Grigoriev, and Mr. Richard Portman for helping with the ICP-MS, XRD, and SEM measurements.

References

[1] Z. Jin, T. Fukumura, M. Kawasaki et al., "High throughput fabrication of transition-metal-doped epitaxial ZnO thin films: a series of oxide-diluted magnetic semiconductors and their properties," *Applied Physics Letters*, vol. 78, no. 24, pp. 3824–3826, 2001.

[2] A. Simimol, A. A. Anappara, and H. C. Barshilia, "Influence of defects on electrical properties of electrodeposited co-doped ZnO nanocoatings," *Materials Research Express*, vol. 4, no. 1, article 015001, 2017.

[3] S. Xu and Z. L. Wang, "One-dimensional ZnO nanostructures: solution growth and functional properties," *Nano Research*, vol. 4, no. 11, pp. 1013–1098, 2011.

[4] A. Simimol, A. A. Anappara, S. Greulich-Weber, P. Chowdhury, and H. C. Barshilia, "Enhanced room temperature ferromagnetism in electrodeposited Co-doped ZnO nanostructured thin films by controlling the oxygen vacancy defects," *Journal of Applied Physics*, vol. 117, no. 21, article 214310, 2015.

[5] L. El Mir, Z. Ben Ayadi, H. Rahmouni, J. El Ghoul, K. Djessas, and H. J. von Bardeleben, "Elaboration and characterization of Co doped, conductive ZnO thin films deposited by radio-frequency magnetron sputtering at room temperature," *Thin Solid Films*, vol. 517, no. 21, pp. 6007–6011, 2009.

[6] F. Ahmed, S. Kumar, N. Arshi, M. S. Anwar, B. H. Koo, and C. G. Lee, "Doping effects of Co^{2+} ions on structural and magnetic properties of ZnO nanoparticles," *Microelectronic Engineering*, vol. 89, pp. 129–132, 2012.

[7] H. Gu, W. Zhang, Y. Xu, and M. Yan, "Effect of oxygen deficiency on room temperature ferromagnetism in Co doped ZnO," *Applied Physics Letters*, vol. 100, no. 20, article 202401, 2012.

[8] B. Pal, S. Dhara, P. K. Giri, and D. Sarkar, "Room temperature ferromagnetism with high magnetic moment and optical properties of Co doped ZnO nanorods synthesized by a solvothermal route," *Journal of Alloys and Compounds*, vol. 615, pp. 378–385, 2014.

[9] S. Benramache and B. Benhaoua, "Influence of annealing temperature on structural and optical properties of ZnO: in thin films prepared by ultrasonic spray technique," *Superlattices and Microstructures*, vol. 52, no. 6, pp. 1062–1070, 2012.

[10] S. Yang, R. Lv, C. Wang, Y. Liu, and Z. Song, "Structural and magnetic properties of cobalt-doped ZnO thin films on sapphire (0 0 0 1) substrate deposited by pulsed laser deposition," *Journal of Alloys and Compounds*, vol. 579, pp. 628–632, 2013.

[11] P. Hari and A. Kaphle, "Cobalt Doped Nanostructured ZnO/p-Si Heterojunctions for Energy Conversion Devices,"

in *Nanomaterials and Nanotechnology*, W. Ahmed, Ed., pp. 74–96, One Central Press, Manchester, 2016.

[12] P. Hari, J. Seay, K. Farmer, and K. Roberts, "Cobalt doped ZnO nanorods fabricated by chemical bath deposition technique," *Advances in Science and Technology*, vol. 77, pp. 280–284, 2012.

[13] K. Farmer, P. Hari, and K. Roberts, "pH study of zinc oxide nanorods grown on indium tin oxide coated substrate," *Canadian Journal of Physics*, vol. 92, no. 7/8, pp. 838–841, 2014.

[14] A. Kaphle and P. Hari, "Characterization of aluminum doped nanostructured ZnO/p-Si heterojunctions," *International Journal of Engineering Science*, vol. 5, pp. 41–51, 2016.

[15] Z. Lin Wang, "Zinc oxide nanostructures: growth, properties and applications," *Journal of Physics: Condensed Matter*, vol. 16, no. 25, article R829, 2004.

[16] F. K. Shan and Y. S. Yu, "Band gap energy of pure and Al-doped ZnO thin films," *Journal of the European Ceramic Society*, vol. 24, no. 6, pp. 1869–1872, 2004.

[17] A. Kaphle and P. Hari, "Variation of index of refraction in cobalt doped ZnO nanostructures," *Journal of Applied Physics*, vol. 122, no. 16, article 165304, 2017.

[18] A. Kaphle and P. Hari, "Enhancement in power conversion efficiency of silicon solar cells with cobalt doped ZnO nanoparticle thin film layers," *Thin Solid Films*, vol. 657, pp. 76–87, 2018.

[19] A. Kaphle, E. Echeverria, D. N. Mcllroy, K. Roberts, and P. Hari, "Thermo-optical properties of cobalt-doped zinc oxide (ZnO) nanorods," *Journal of Nanoscience and Nanotechnology*, vol. 19, no. 7, pp. 3893–3904, 2019.

[20] A. Kaphle, M. F. Borunda, and P. Hari, "Influence of cobalt doping on residual stress in ZnO nanorods," *Materials Science in Semiconductor Processing*, vol. 84, pp. 131–137, 2018.

[21] R. Ma, Z. Liu, K. Takada et al., "Tetrahedral Co(II) coordination in α-type cobalt hydroxide: Rietveld refinement and X-ray absorption spectroscopy," *Inorganic Chemistry*, vol. 45, no. 10, pp. 3964–3969, 2006.

[22] A. G. Blackman, *Encycl. Inorg. Chem.*, John Wiley & Sons, Ltd, Chichester, UK, 2006.

[23] C. Verrier, E. Appert, O. Chaix-Pluchery et al., "Effects of the pH on the formation and doping mechanisms of ZnO nanowires using aluminum nitrate and ammonia," *Inorganic Chemistry*, vol. 56, no. 21, pp. 13111–13122, 2017.

[24] J. Joo, B. Y. Chow, M. Prakash, E. S. Boyden, and J. M. Jacobson, "Face-selective electrostatic control of hydrothermal zinc oxide nanowire synthesis," *Nature Materials*, vol. 10, no. 8, pp. 596–601, 2011.

[25] H. Cui, Y. Zhao, W. Ren, M. Wang, and Y. Liu, "Large scale selective synthesis of α-$Co(OH)_2$ and β-$Co(OH)_2$ nanosheets through a fluoride ions mediated phase transformation process," *Journal of Alloys and Compounds*, vol. 562, pp. 33–37, 2013.

[26] C. Verrier, E. Appert, O. Chaix-Pluchery et al., "Tunable morphology and doping of ZnO nanowires by chemical bath deposition using aluminum nitrate," *Journal of Physical Chemistry C*, vol. 121, no. 6, pp. 3573–3583, 2017.

[27] N. Winkler, S. Edinger, W. Kautek, and T. Dimopoulos, "Mg-doped ZnO films prepared by chemical bath deposition," *Journal of Materials Science*, vol. 53, no. 7, pp. 5159–5171, 2018.

[28] G. C. Park, S. M. Hwang, J. H. Lim, and J. Joo, "Growth behavior and electrical performance of Ga-doped ZnO nanorod/p-Si heterojunction diodes prepared using a hydrothermal method," *Nanoscale*, vol. 6, no. 3, pp. 1840–1847, 2014.

[29] K. M. McPeak, T. P. Le, N. G. Britton, Z. S. Nickolov, Y. A. Elabd, and J. B. Baxter, "Chemical bath deposition of ZnO nanowires at near-neutral pH conditions without hexamethylenetetramine (HMTA): understanding the role of HMTA in ZnO nanowire growth," *Langmuir*, vol. 27, no. 7, pp. 3672–3677, 2011.

[30] M. N. R. Ashfold, R. P. Doherty, N. G. Ndifor-Angwafor, D. J. Riley, and Y. Sun, "The kinetics of the hydrothermal growth of ZnO nanostructures," *Thin Solid Films*, vol. 515, no. 24, pp. 8679–8683, 2007.

[31] K. Govender, D. S. Boyle, P. B. Kenway, and P. O'Brien, "Understanding the factors that govern the deposition and morphology of thin films of ZnO from aqueous solution," *Journal of Materials Chemistry*, vol. 14, no. 16, pp. 2575–2591, 2004.

[32] S. Peulon and D. Lincot, "Mechanistic study of cathodic electrodeposition of zinc oxide and zinc hydroxychloride films from oxygenated aqueous zinc chloride solutions," *Journal of the Electrochemical Society*, vol. 145, no. 3, p. 864, 1998.

[33] D. Pradhan and K. T. Leung, "Controlled growth of two-dimensional and one-dimensional ZnO nanostructures on indium tin oxide coated glass by direct electrodeposition," *Langmuir*, vol. 24, no. 17, pp. 9707–9716, 2008.

[34] D. Pradhan and K. T. Leung, "Vertical growth of two-dimensional zinc oxide nanostructures on ITO-coated glass: effects of deposition temperature and deposition time," *Journal of Physical Chemistry C*, vol. 112, no. 5, pp. 1357–1364, 2008.

[35] H. M. Cheng, W. H. Chiu, C. H. Lee, S. Y. Tsai, and W. F. Hsieh, "Formation of branched ZnO nanowires from solvothermal method and dye-sensitized solar cells applications," *The Journal of Physical Chemistry C*, vol. 112, no. 42, pp. 16359–16364, 2008.

[36] J. Qiu, M. Guo, and X. Wang, "Electrodeposition of hierarchical ZnO nanorod-nanosheet structures and their applications in dye-sensitized solar cells," *ACS Applied Materials & Interfaces*, vol. 3, no. 7, pp. 2358–2367, 2011.

[37] A. Smith and R. Rodriguez-Clemente, "Morphological differences in ZnO films deposited by the pyrosol technique: effect of HCl," *Thin Solid Films*, vol. 345, no. 2, pp. 192–196, 1999.

[38] Y. L. Xie, J. Yuan, P. Song, and S. Q. Hu, "Growth of ZnO nanorods and nanosheets by electrodeposition and their applications in dye-sensitized solar cells," *Journal of Materials Science: Materials in Electronics*, vol. 26, no. 6, pp. 3868–3873, 2015.

[39] J. Sithole, B. D. Ngom, S. Khamlich et al., "Simonkolleite nanoplatelets: synthesis and temperature effect on hydrogen gas sensing properties," *Applied Surface Science*, vol. 258, no. 20, pp. 7839–7843, 2012.

[40] A. Bora and K. C. Sarma, "A temperature modulation circuit for metal oxide semiconductor gas sensor," *Indian Journal of Science and Technology*, vol. 8, no. 12, 2015.

[41] J. L. Noel, R. Udayabhaskar, B. Renganathan, S. Muthu Mariappan, D. Sastikumar, and B. Karthikeyan, "Spectroscopic and fiber optic ethanol sensing properties Gd doped ZnO nanoparticles," *Spectrochimica Acta Part A: Molecular and Biomolecular Spectroscopy*, vol. 132, pp. 634–638, 2014.

[42] G. Xiong, U. Pal, J. G. Serrano, K. B. Ucer, and R. T. Williams, "Photoluminesence and FTIR study of ZnO nanoparticles: the

impurity and defect perspective," *Physica Status Solidi (c)*, vol. 3, no. 10, pp. 3577–3581, 2006.

[43] P. V. Kamat, N. M. Dimitrijevic, and A. J. Nozik, "Dynamic Burstein-Moss shift in semiconductor colloids," *The Journal of Physical Chemistry*, vol. 93, no. 8, pp. 2873–2875, 1989.

[44] D. Y. Kim, S.-O. Kim, M. S. Kim et al., "Hydrothermal growth and properties of rod-like ZnO submicron crystals on Al-doped ZnO seed layers with different Al concentrations," *Journal of the Korean Physical Society*, vol. 60, no. 1, pp. 94–98, 2012.

[45] J. J. Beltrán, C. A. Barrero, and A. Punnoose, "Combination of defects plus mixed valence of transition metals: a strong strategy for ferromagnetic enhancement in ZnO nanoparticles," *Journal of Physical Chemistry C*, vol. 120, no. 16, pp. 8969–8978, 2016.

[46] K. J. Kim and Y. R. Park, "Spectroscopic ellipsometry study of optical transitions in Zn1−xCoxO alloys," *Applied Physics Letters*, vol. 81, no. 8, pp. 1420–1422, 2002.

[47] M. Bouloudenine, N. Viart, S. Colis, and A. Dinia, "Bulk Zn1 −xCoxO magnetic semiconductors prepared by hydrothermal technique," *Chemical Physics Letters*, vol. 397, no. 1-3, pp. 73–76, 2004.

[48] S. V. Bhat and F. L. Deepak, "Tuning the bandgap of ZnO by substitution with Mn^{2+}, Co^{2+} and Ni^{2+}," *Solid State Communications*, vol. 135, no. 6, pp. 345–347, 2005.

[49] X.-C. Liu, E.-W. Shi, Z.-Z. Chen et al., "Structural, optical and magnetic properties of Co-doped ZnO films," *Journal of Crystal Growth*, vol. 296, no. 2, pp. 135–140, 2006.

[50] M. Ivill, S. J. Pearton, S. Rawal et al., "Structure and magnetism of cobalt-doped ZnO thin films," *New Journal of Physics*, vol. 10, no. 6, article 065002, 2008.

[51] I. Ozerov, F. Chabre, and W. Marine, "Incorporation of cobalt into ZnO nanoclusters," *Materials Science and Engineering: C*, vol. 25, no. 5-8, pp. 614–617, 2005.

[52] Y.-Z. Yoo, T. Fukumura, Z. Jin et al., "ZnO–CoO solid solution thin films," *Journal of Applied Physics*, vol. 90, no. 8, pp. 4246–4250, 2001.

[53] J.-M. Myoung, W.-H. Yoon, D.-H. Lee, I. Yun, S.-H. Bae, and S.-Y. Lee, "Effects of thickness variation on properties of ZnO thin films grown by pulsed laser deposition," *Japanese Journal of Applied Physics*, vol. 41, no. 1, Part 1, pp. 28–31, 2002.

[54] D. Verma, A. K. Kole, and P. Kumbhakar, "Red shift of the band-edge photoluminescence emission and effects of annealing and capping agent on structural and optical properties of ZnO nanoparticles," *Journal of Alloys and Compounds*, vol. 625, pp. 122–130, 2015.

[55] R. K. Sendi and S. Mahmud, "Stress control in ZnO nanoparticle-based discs via high-oxygen thermal annealing at various temperatures," *Journal of Physical Science*, vol. 24, no. 1, p. 1, 2013.

[56] A. Ghosh, N. Karak, and T. K. Kundu, "Effect of Co doping on optical behaviors in ZnO nanorods," in *Proceedings of International Conference on Recent Trends in Applied Physics & Materials Science : RAM 2013*, Bikaner, Rajasthan, India, 2013.

[57] Q. Xiao, J. Zhang, C. Xiao, and X. Tan, "Photocatalytic decolorization of methylene blue over $Zn_{1-x}Co_xO$ under visible light irradiation," *Materials Science and Engineering B*, vol. 142, no. 2-3, pp. 121–125, 2007.

[58] P. K. Sharma, R. K. Dutta, and A. C. Pandey, "Alteration of magnetic and optical properties of ultrafine dilute magnetic semiconductor ZnO:Co^{2+} nanoparticles," *Journal of Colloid and Interface Science*, vol. 345, no. 2, pp. 149–153, 2010.

[59] S. Rahmane, M. S. Aida, M. A. Djouadi, and N. Barreau, "Effects of thickness variation on properties of ZnO:Al thin films grown by RF magnetron sputtering deposition," *Superlattices and Microstructures*, vol. 79, pp. 148–155, 2015.

[60] Z.-H. Wu, H.-Q. Xie, and Y.-B. Zhai, "Preparation and thermoelectric properties of Co-doped ZnO synthesized by sol–gel," *Journal of Nanoscience and Nanotechnology*, vol. 15, no. 4, pp. 3147–3150, 2015.

[61] S. K. Saha, M. A. Rahman, M. R. H. Sarkar, M. Shahjahan, and M. K. R. Khan, "Effect of Co doping on structural, optical, electrical and thermal properties of nanostructured ZnO thin films," *Journal of Semiconductors*, vol. 36, no. 3, article 033004, 2015.

[62] M. M. Rahman, M. K. R. Khan, M. R. Islam et al., "Effect of Al doping on structural, electrical, optical and photoluminescence properties of nano-structural ZnO thin films," *Journal of Materials Science and Technology*, vol. 28, no. 4, pp. 329–335, 2012.

[63] A. A. Yousif, N. F. Habubi, and A. A. Haidar, "Nanostructure Zinc Oxide with Cobalt Dopant by PLD for Gas Sensor Applications," *Journal of Nano- and Electronic Physics*, vol. 4, article 02007, 2012.

[64] R. Kumar and N. Khare, "Temperature dependence of conduction mechanism of ZnO and Co-doped ZnO thin films," *Thin Solid Films*, vol. 516, no. 6, pp. 1302–1307, 2008.

[65] B. Van Zeghbroeck, *Principles of Semiconductor Devices*, University of Colorado, Boulder, CO, USA, 2011.

[66] S. Hussain, *Investigation of Structural and Optical Properties of Nanocrystalline ZnO*, Linkoping University, 2008.

[67] Y. Wu, S. E. Potts, P. M. Hermkens, H. C. M. Knoops, F. Roozeboom, and W. M. M. Kessels, "Enhanced doping efficiency of Al-doped ZnO by atomic layer deposition using dimethylaluminum isopropoxide as an alternative aluminum precursor," *Chemistry of Materials*, vol. 25, no. 22, pp. 4619–4622, 2013.